Forces in Mechanics 6 (2022) 100073

Contents lists available at ScienceDirect

Forces in Mechanics

journal homepage: www.sciencedirect.com/journal/forces-in-mechanics

Determination of residual stress evolution during repair welding of high-strength steel components

Becker Amadeus [a,*], Schroepfer Dirk [a], Kromm Arne [a], Kannengiesser Thomas [a,b]

[a] Bundesanstalt für Materialforschung und -prüfung (BAM), Berlin, Germany
[b] Otto-von-Guericke University, Magdeburg, Germany

ARTICLE INFO

Key words:
Repair-welding
High-strength steels
X-ray diffraction
Digital image correlation
Residual stresses

ABSTRACT

During the assembly of steel structures, unacceptable weld defects may be found. An economical solution is local thermal gouging of the affected areas and re-welding. Due to high shrinkage restraints of repair weld and surrounding structure, high global and local welding stresses superimpose, and may lead to cracking and component failure, especially in connection with the degraded microstructure and mechanical properties of high-strength steels during the repair process. Component-related investigations of high-strength steels (FOSTA P1311/IGF20162N) focus on welding residual stress evolution during local thermal gouging and rewelding. In this study, repair welding of S500MLO (EN 10225) is carried out using in-situ digital image correlation (DIC) and ex-situ X-ray diffraction (XRD) to analyse strains and stresses. Self-restrained slit specimen geometries were identified representing defined rigidity conditions of repair welds of real components, which were quantified using the restraint intensity concept. The specimens were rewelded with constant welding heat control and parameters. Weld specimens exhibited significantly increased transverse residual stresses with higher transverse restraint intensities, in the weld metal, and in the heat affected zone. Transverse stresses along the weld seam decrease at the weld seam ends leading to different stress state during gouging and welding. XRD analysis of the longitudinal and transverse local residual stresses after cooling to RT showed a good comparability with global DIC analyses.

1. Introduction

The sustainable and resource-efficient production of wind energy plants requires the use of modern high-strength fine-grain structural steels. This applies to both foundation and erection structures. Depending on the application, manufacturers and operators of structures made of high-strength structural steels [1] have to meet high requirements in terms of weld joint safety and quality in accordance with the relevant standards [2]. This involves a continuous non-destructive testing of the welds during the manufacturing process for approval and in the further life cycle. If critical defects and imperfections are found, there is the option of local gouging of the defective areas with subsequent repair welding of the groove. Deeper weld defects are usually gouged by thermal methods, such as carbon arc gouging, due to economic aspects and advantages regarding crack detection, where the weld metal is melted by means of a graphite electrode and the slag is blown out by means of compressed air [3], as shown in Fig. 1a. The resulting groove can be repair welded after appropriate reworking. In practice, decisions on the feasibility of a safe repair weld as well as on the procedure are mostly based on empirical values and the know-how of the manufacturing companies. Standards and guidelines for welding processing, especially in the case of high-strength steels, do not provide specific advice and information on adequate repair concepts.

The applied thermal gouging processes and repeated welding cause thermo-mechanical stresses and microstructure degradation in the original welded joint. Thus, a disproportionate degradation of the microstructure is to be expected as a result of repeated thermal stresses if more than one repair cycles are necessary. Thermal gouging involves very high heating and cooling rates and can lead to significant ductility and toughness losses, especially in multilayer welds in the areas of the heat-affected zone (HAZ) when repeatedly heated to peak temperatures between Ac1 and Ac3 [4], the intercritical heated partially austenitised range. At temperatures just above the Ac1 temperature, the carbon enriched microstructural components transform into austenite. A high cooling rate would result in carbon enriched martensite or bainite. Thus, with increasing number of repair cycles, increasing microstructure degradation is to be expected [3]. Furthermore, the use of graphite electrodes in gouging leads to carbon enrichment at the seam edges,

* Corresponding author.
E-mail address: Amadeus.Becker@bam.de (B. Amadeus).

https://doi.org/10.1016/j.finmec.2022.100073
Received 12 November 2021; Received in revised form 7 January 2022; Accepted 16 January 2022
Available online 18 January 2022

which according to Karpenko [5] can be up to 2% in the surface of the gouged groove.

In addition, the weld-related stresses in the repair weld are usually higher than in the original weld, since the welding of the gouged grooves in the overall structure is subject to increased restraint conditions [1]. Welding causes transient and permanent stresses depending on the material used, the welding process and the constructive shrinkage restraint [4]. Locally in the weld area, residual stresses - the so-called restraint stresses - are the result of temporally and locally inhomogeneous elastic and plastic deformations due to thermal shrinkage, solid phase transformation and quenching processes and ultimately a complex superposition of these effects [6–8], as schematically shown in Fig. 1b. In the case of component welds, additional design-related shrinkage restraints are present, which additionally lead to reaction forces and stresses at the weld cross-section and are superimposed with the local restraint stresses, cf. Fig. 1c [9]. Especially in the case of the usually slit-shaped repair welds, high design stiffnesses are to be expected, cf. Fig. 1a. As a result, high additional tensile residual stresses are initiated which may be crack critical in combination with a degraded microstructure.

An approach to quantify the restraint situation during repair welding is the restraint intensity model according to Satoh [10,11]. The restraint intensity is based on an analytical transverse shrinkage force model, where within the elastic range of the base material the transverse shrinkage force F_y is related to the overall transverse shrinkage ($\Delta y = \Delta y_1 + \Delta y_2$) and the weld length L_S. Furthermore, the restraint intensity can be described according to Hooke's law with the Young's modulus E and the plate thickness H:

$$R_{Fy} = (E{\cdot}H)/L_S = F_y/((\Delta y_1 + \Delta y_2){\cdot}L_S)\,inkN{\cdot}(mm{\cdot}mm)^{-1} \quad (1)$$

This makes it possible both to quantify the shrinkage restraints of real component and repair weld details and to compare them with each other and transfer them to near-component test setups. Numerous investigations based on different test conditions showed that the residual stresses that arise are clearly dependant on the level of shrinkage restraint and that the expected stress level can be estimated with sufficient accuracy using the restraint intensity concept [12,7]. Analyses of the dependence of the degree of restraint and the weld heat transfer showed significant effects of these parameters on the hindrance of transverse shrinkage. In particular, it was shown that low interpass temperatures and a preferential setting of the cooling times by adjusting the heat input and heat input may be helpful to significantly reduce the stress level after welding and cooling, especially under high stiffness conditions [8]. However, this has not yet been systematically investigated for repair welding situations.

2. General approach and procedure

Against this background, a current research project of BAM (FOSTA P1311/IGF-No. 20162N) focuses on the welding of structural component-like specimens which specifically represent realistic support and heat dissipation conditions of repair welds. In a first step, self-restrained specimen shapes were identified for this purpose applying the restraint intensity model according to Satoh [10,11]. The approach applied was to use slit specimens with specific external dimensions, whereas the restraint intensity is adjusted by varying the slit lengths L_S. Various studies have already shown a number of correlations, e.g., on the basis of different slit specimen configurations and the transferability of these from laboratory scale to full-scale component dimensions with the aid of experiments on large-scale testing facilities [13,14,7] as well as approaches for predicting residual stresses on the basis of numerical simulations taking into account the component and weld geometry [15, 16].

By means of structural simulation, the restraint intensities of about $R_{Fy} = 11$ kN•(mm•mm)$^{-1}$ ($L_S = 200$ mm) and 22 kN•(mm•mm)$^{-1}$ ($L_S = 125$ mm) could be determined for the selected specimens, cf. Fig. 2a,b. Due to the specimen symmetry, it was possible to use a half-model and to block all degrees of freedom at the axis of symmetry in the centre of the specimen, as shown in Fig. 2c. The meshing of the model was accomplished in respect of the further investigation of large-scale component structures with shell elements, whereby the element size was successively adjusted. Previous numerical and experimental analyses [7, 13-15] show good comparability of the results and a small influence of the seam preparation at high surrounding stiffness, so that the V-seam preparation could be idealized as an I-seam by using shell elements. The restraint intensity is calculated analogously to [8,13] by applying a surface load of 100 MPa at $E = 215$ GPa and calculating the resulting displacement of the weld flanks $\Delta 2y$ over the slit length, cf. Fig. 2c. A free-shrinking specimen with no restraint transverse to the weld direction ("0 kN•(mm•mm)$^{-1}$") was chosen as a reference. The three specimen shapes thus represent repair cases under free shrinkage (specimen P1), medium (slit specimen P2: $L_S = 200$ mm) and high shrinkage restraint (slit specimen P3: $L_S = 125$ mm) and were mechanically manufactured. Welding experiments were performed on all specimen shapes, using in-situ measurement methods to determine the occurring transient displacements and stresses during welding, cf. Section 2.1. After cooling to ambient temperature, residual stress measurements were performed to quantify residual stresses for corresponding shrinkage restraint conditions after repair welding, cf. Section 2.2.

2.1. Welding experiments with in-situ DIC analyses

The MAG welding experiments were carried out on the material S500MLO (EN 10225) with the solid wire filler metal G50 7 M21 4Mo (ISO 12341) under free-shrinking and restrained conditions ((0; 11; 12) kN•(mm•mm)$^{-1}$). The chemical composition and mechanical properties of the base materials and filler metals are listed in Table 1. Using a linear axis, cf. Fig. 3a, constant welding parameters were realized for all

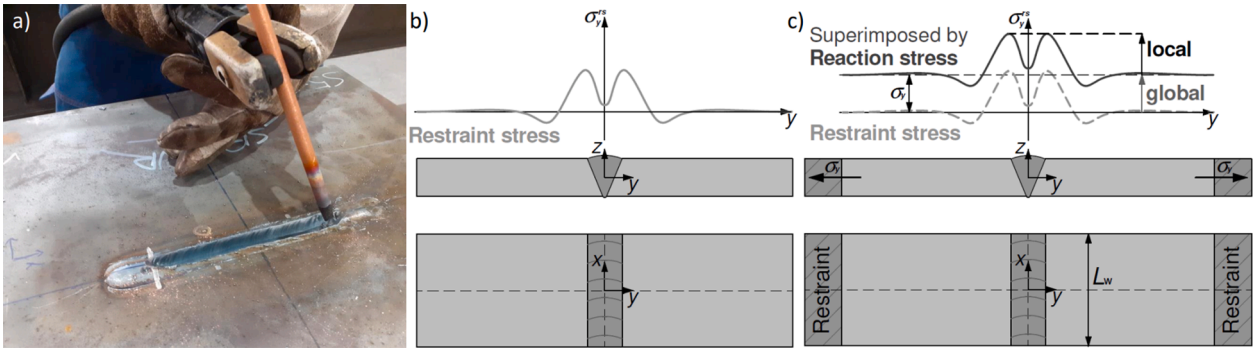

Fig. 1. (a) Groove after gouging with carbon electrode; (b) schematic illustration of local restraint stresses under free-shrinking conditions and (c) superposition of the local residual stresses and global reaction stresses [8].

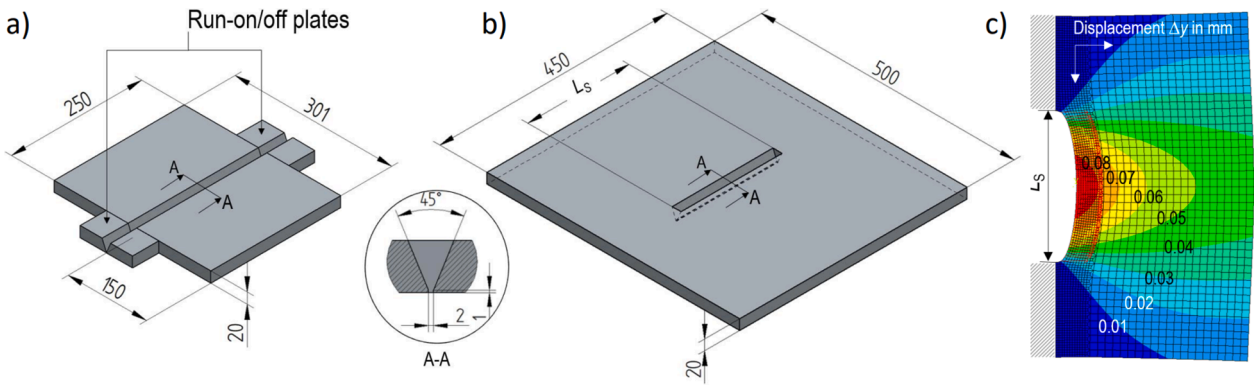

Fig. 2. (a) Free-shrinking specimen P1, (b) self-restrained slit specimens with varied slit-length P2 (L_S = 200 mm) and P3 (L_S = 125 mm), (c) numeric modelling.

Table 1
Chemical composition of base material, filler material and mechanical properties (at room temperature).

Base / filler material in wt.-%	C	Si	Mn	Cr	Mo	Nb	Ni	$R_{p0,2}$	R_m	A_5	Av
S500MLO (EN 10225)	0.053	0.34	1.81	0.17	0.13	0.040	0.110	546 MPa	736 MPa	22%	324 J @ −40 °C
G 50 7 M21 4Mo (ISO 12341)	0.100	0.69	1.82	0.03	0.43	0.002	0.020	607 MPa	637 MPa	18%	60 J @ −70 °C

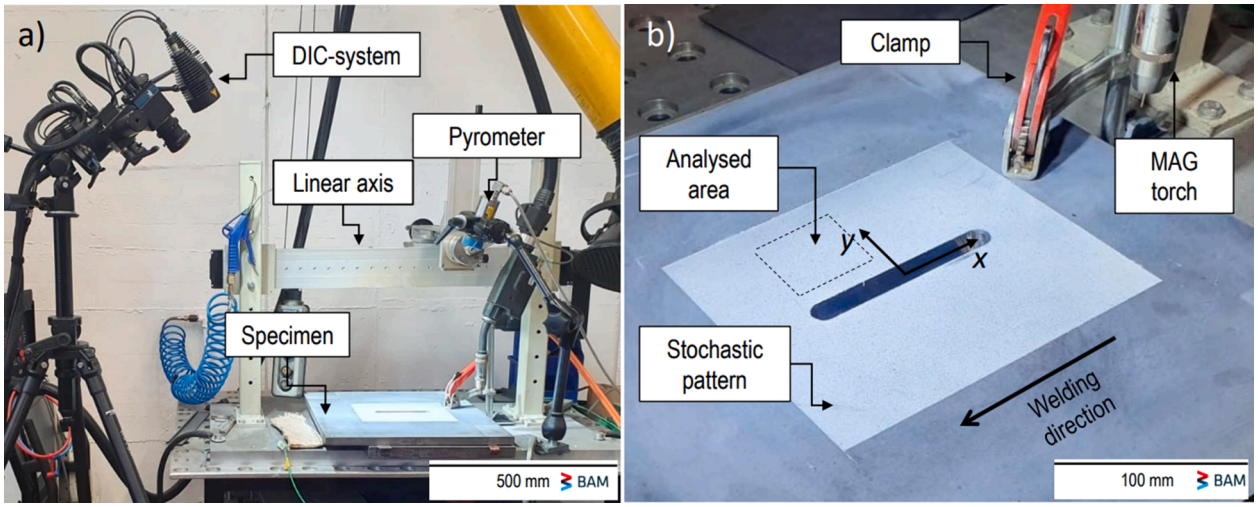

Fig. 3. (a) Test setup welding experiments, (b) close-up prepared specimen with DIC-area.

specimens and experiments, as listed in Table 2. Prior to welding, the specimens were preheated using locally at the slit to 50 °C. The interpass temperature during welding was monitored using thermocouples. A pyrometer (measuring range: 150 to 1500 °C) was used to determine the $\Delta t_{8/5}$ cooling times on the weld bead. By using a digital image correlation (DIC) system, an in-situ 2-dimensional measurement of the transient strains and displacements occurring during welding and cooling was performed. For this purpose, the specimens were previously prepared with a stochastic pattern, as shown in Fig. 3b.

2.2. Ex-situ XRD analysis

The resulting residual stresses were measured by X-ray diffraction (XRD) [17]. Two systems were used for this purpose: On a selected slit specimen (P3: L_S = 125 mm), the transverse, longitudinal and shear stresses were measured 2-dimensionally over the specimen surface using a robotic system. The residual stresses were determined applying a linear least square analysis of the $\sin^2\Psi$-law (Dölle-Hauk equation) by using 19 Ψ (−45° to 45°) and 3 φ (0, 60°, 120°) tilts each. For the large number of the different specimens, the transverse residual stresses were analysed along a measuring track transverse to the welding direction (up to ±100 mm from the weld centre). Here, a semi-automatic measuring system was used, applying the $\sin^2\Psi$-method (CrKα; collimator: D = 2 mm; Ψ-steps: 7; Ψ-range: ±45°).

Table 2
Welding parameters and test variation.

Welding current/ voltage	Welding speed	Wire feed speed	Preheat/interpass temperature	Heat input	$\Delta t_{8/5}$ cooling time	Restraint intensities R_{Fy} in kN•(mm•mm)$^{-1}$
261 A / 25.5 V	26 cm/min	8.5 m/min	50 °C / ~150 °C	1.6 kJ/mm	Ø 13.7 s	0; 11; 22

3. Results

3.1. Effect of the transverse restraint intensity on welding stresses

Fig. 4a shows the transverse residual stress distribution across the weld seam of the free-shrinking specimen (P1). It shows a typical residual stress profile for a transformable steel according to the established models [4, 6,18,19]. The tensile residual stress maxima are located in the weld metal near the weld seam transition being up to approx. 200 MPa. Farther away from the transition to the weld centre, low tensile residual stresses of up to 50 MPa and down to residual compressive stresses of −100 MPa are present. These compressive residual stresses are mainly caused by superposition with transformation residual stresses due to volume expansion during the transformation from austenite to ferrite while cooling. The secondary maxima of the tensile residual stresses in the free-shrinking welded specimen occur in the HAZ up to about 150 MPa. Starting from the HAZ in the direction of the base metal, the residual stresses drop to the initial state of around 0 MPa.

The slit specimens, on the other hand, show significantly increased residual stress profiles, as shown in Fig. 4b. The design-related shrinkage restraint initiates reaction forces which, causing – even in the far field of the weld – still significantly higher transverse residual stresses compared to the initial stress state of the surface before welding. At a distance of 60 mm from the centre of the weld, these are still at approx. 100 MPa at the medium restraint (P2) and 120 MPa at the upper restraint level (P3). In addition, a significant increase in the tensile residual stress maxima can be observed in the HAZ, resulting from the complex superposition with the reaction stresses due to the restraint condition [8]. For the long-slit weld (P2), the tensile residual stress maximum at the HAZ is approx. 300 MPa and for the short-slit weld it is almost 400 MPa, which corresponds to approx. 80% of the nominal yield strength of the base metal. Due to the superposition of the global reaction and local welding stresses, the weld metal and weld transition regions also show significantly elevated residual stress level compared to the free-shrinkage weld specimen (P1). The evaluation of the averaged residual stress indicates a continuous increase in the stress level with the restraint intensity for both the weld metal and the HAZ, see Fig. 4c. It should be emphasized that the stress level in the HAZ is increased by about 100 MPa at the high restraint intensity (R_{Fy} = 22 N•(mm•mm)$^{-1}$) compared to the weld metal, being almost at 60% of the nominal yield strength. This could be especially critical, since the HAZ could show significant microstructural degradation due to gouging and repair welding.

3.2. 2-dimensional ex-situ XRD analysis of highly restrained welds

The residual stresses on the surfaces at and around the highly restrained weld (P3, L_S = 125 mm) were additionally determined by means of XRD 2-dimensional analysis and are shown as stress maps in transverse and longitudinal direction in Fig. 5a,b. Furthermore, Fig. 5c exhibits the map of residual shear stresses. Compared to the stress profiles shown in Fig. 4 the superposition of the local restraint stresses of the weld and global reaction stresses adjacent to the weld is also obvious, cf. Fig. 6b. Maxima of the transverse residual stresses are located in the centre of the specimen and the weld, while compressive residual stresses are found in the areas of weld start and end. This is also obvious in Fig. 6a, showing a transverse stress profile of a measuring track along the weld adjacent the weld seam (y = 13 mm). Tensile transverse residual stresses still exhibit at a distance of 100 mm from the weld centre line, cf. Fig 5a. The longitudinal residual stresses also increase in the direction towards the centre of the weld, cf. Fig. 5b and Fig. 6b, showing tensile values over the whole weld seam. Herein, a high local maximum of up to 450 MPa occurs in the HAZ 1 mm to 2 mm adjacent to the transition to the weld metal. At a distance of approx. 30 mm from the weld centre line (at x = 0 mm), the longitudinal stresses decrease to compressive values of approx. -50 MPa. The map of the shear residual stresses indicates a transition from a maximum at the weld end to minimum residual shear stresses at the weld start, cf. Fig. 5c, which is also obvious at the residual stress profile at y = 13 mm, cf. Fig 6b.

3.3. 2d in-situ DIC analysis of highly restrained welds

For the specimen under high shrinkage restraint (P3, L_S = 125 mm), the 2-dimensional analysis of displacements and strains on the surface during welding (after 1st layer, 150 °C; 6th (last) layer, 150 °C) until complete cooling were performed in-situ by means of DIC measurements within a selected area (Fig. 3b). As the number of weld beads and heat input accordingly increases during the welding process, transverse displacements increase in the positive direction due to thermal expansion (Fig. 7a,b). In this case, strain maxima of up to 0.2% are reached adjacent to the weld. Due to heat dissipation conditions and increased stiffness towards weld seam start and end, maximum strain is located around the weld/specimen centre line. As the weld cools down to ambient temperature, the strains decrease due to shrinkage and the displacements increase to maximum values especially adjacent to weld around the specimen centre line.

With the average remaining strain within a range of 20 mm distance transverse to the weld direction, a transverse residual stress of $\sigma^{rs}_y \approx$ 150 MPa was calculated (Young's modulus E = 215 GPa, Poisson's ratio ν = 0.3). The results are accordingly (±50 MPa) to the residual stress analysis by means of XRD in the same area, cf. Figs. 5a and 6, and are also in good agreement with recent analyses of comparable weld tests of slit weld specimens [15]. Correlation of the strain and residual stress gradients of the respective maps reveal a good qualitative and quantitative agreement. Hence, it is assumed that in-situ DIC methods by

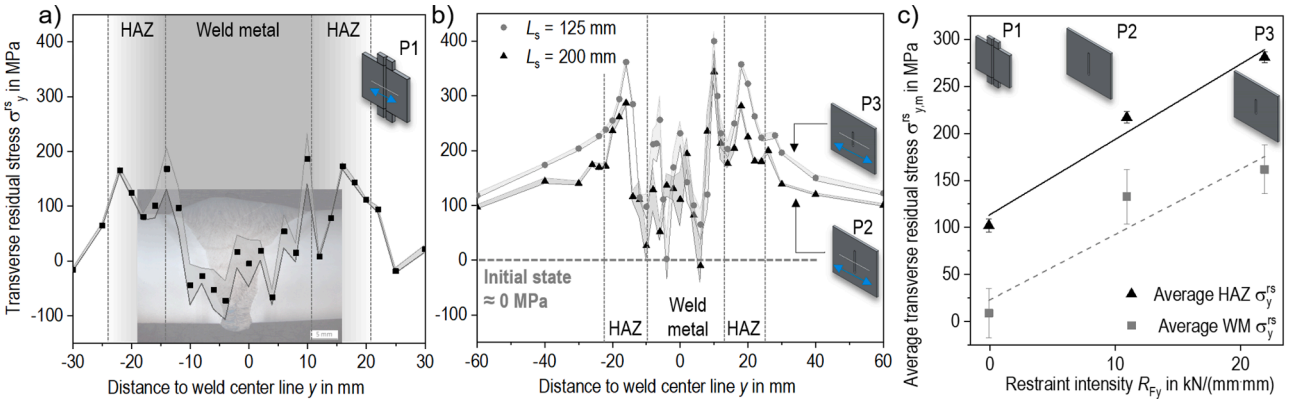

Fig. 4. Transverse residual stress-profiles for (a) free-shrinking specimen P1 and (b) restrained slit specimen P2/P3, (c) restraint intensity VS average transverse residual stresses for HAZ and WM.

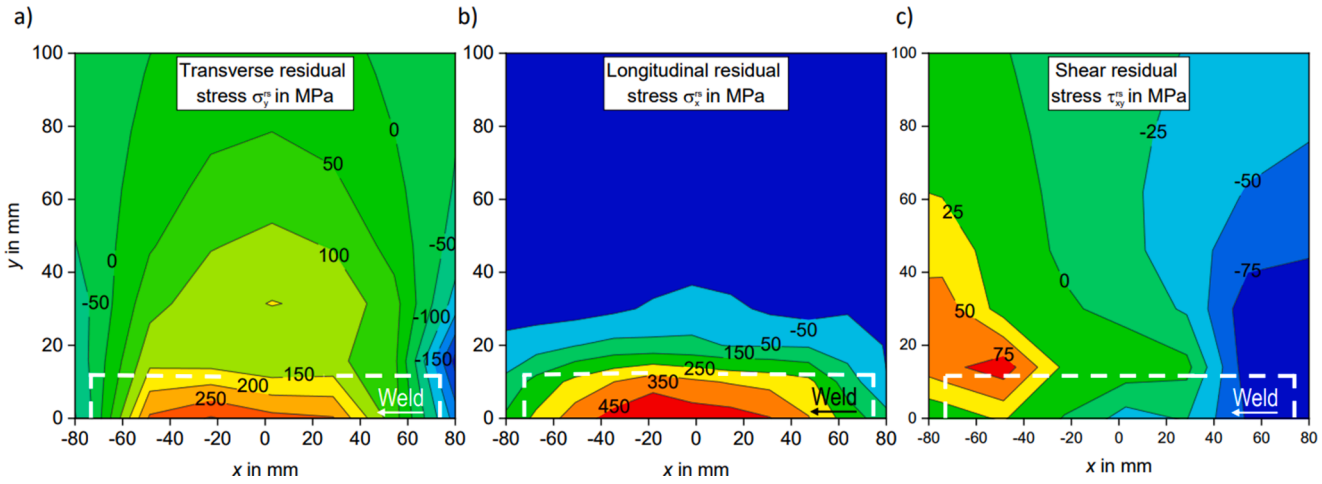

Fig. 5. (a) Transverse, (b) longitudinal and (c) shear residual stresses mapped on specimen surface.

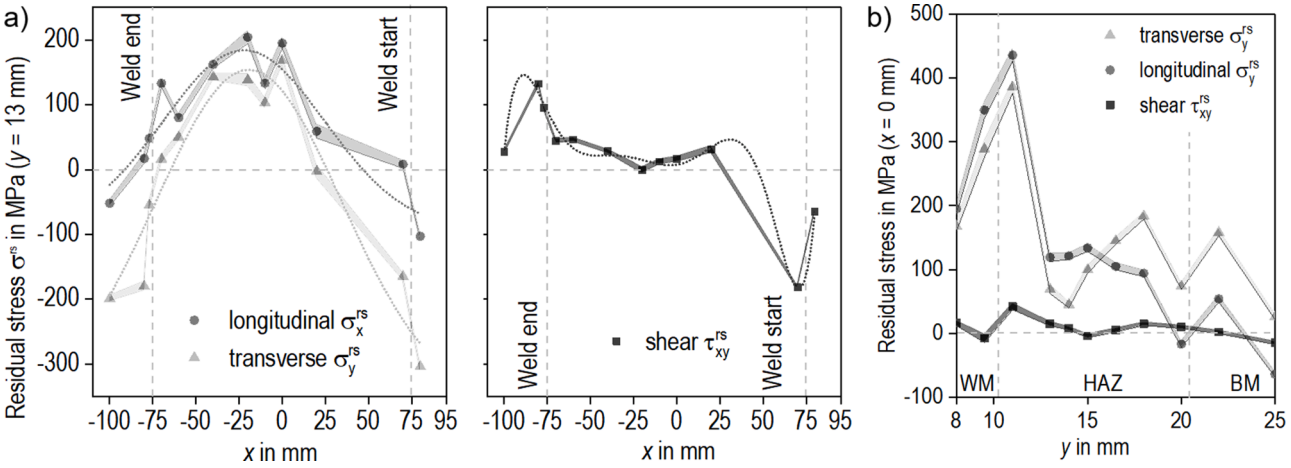

Fig. 6. (a) Transverse, longitudinal and shear residual stress-profiles at measuring track at $y = 13$ mm, (b) Transverse, longitudinal, and shear residual stress-profiles at measuring track at $x = 0$ mm.

means of 2d analysis of displacements and strains are highly suitable to characterize the material response during multilayer welding of highly restraint repair welds. Further DIC investigations should focus on the quantification and comparison of transient strains in the weld area for optimization of repair welding and heat control concepts.

4. Conclusions

Currently, processing regulations provide hardly any information on the welding repair of joints made of high-strength fine-grained structural steels. With regard to their special microstructure and low ductility reserves, high mechanical welding stresses during and after repair welding of joint grooves should be avoided despite the high restraint nature of repair weld situations. With the aim of designing weld tests for the development of adequate repair concepts, welding experiments and corresponding ex-situ and in-situ stress-strain analyses were presented in this study using a high-strength steel S500MLO. The following conclusions can be derived:

- By means of restraint intensity analyses, the identification of specimen shapes can be achieved to represent repair conditions for welding experiments under systematic variation of realistic shrinkage restraints.
- Using digital image correlation, the evaluation of strains due to welding and cooling could be determined in-situ in order to avoid critical transient stresses by an adapted heat control. The results after cooling to ambient temperature are in accordance with residual stress analyses using X-ray diffraction and other studies [15].
- X-ray diffraction analyses show the superposition of local restraint stresses and global reaction stresses. Hence, stepwise increasing of the restraint intensity causes considerable elevation of the transverse residual stress level in the weld seam and adjacent to the weld seam in the heat affected zone.
- The highest transverse residual stress level was found in the HAZ, which is most crack critical due to potentially local degraded microstructure caused by welding, thermal gouging and repair welding. A restraint intensity transverse to the welding direction of RFy = 22 kN.(mm.mm)−1 already causes maximum tensile residual stresses of up to 80% of the nominal material's yield strength.
- High stresses should be avoided by enable lower restraint conditions using adequate repair strategies and welding sequences. If this is not possible at all, in accordance with other studies [8,9,15], welding stresses should be controlled using adapted heat control concepts.

The ultimate aim of these investigations is to transfer the results and findings to real components in both the mobile crane and offshore sectors by means of demonstrator tests and by recommendations for appropriate repair concepts regarding stresses and material degradation as a basis for corresponding standards and guidelines.

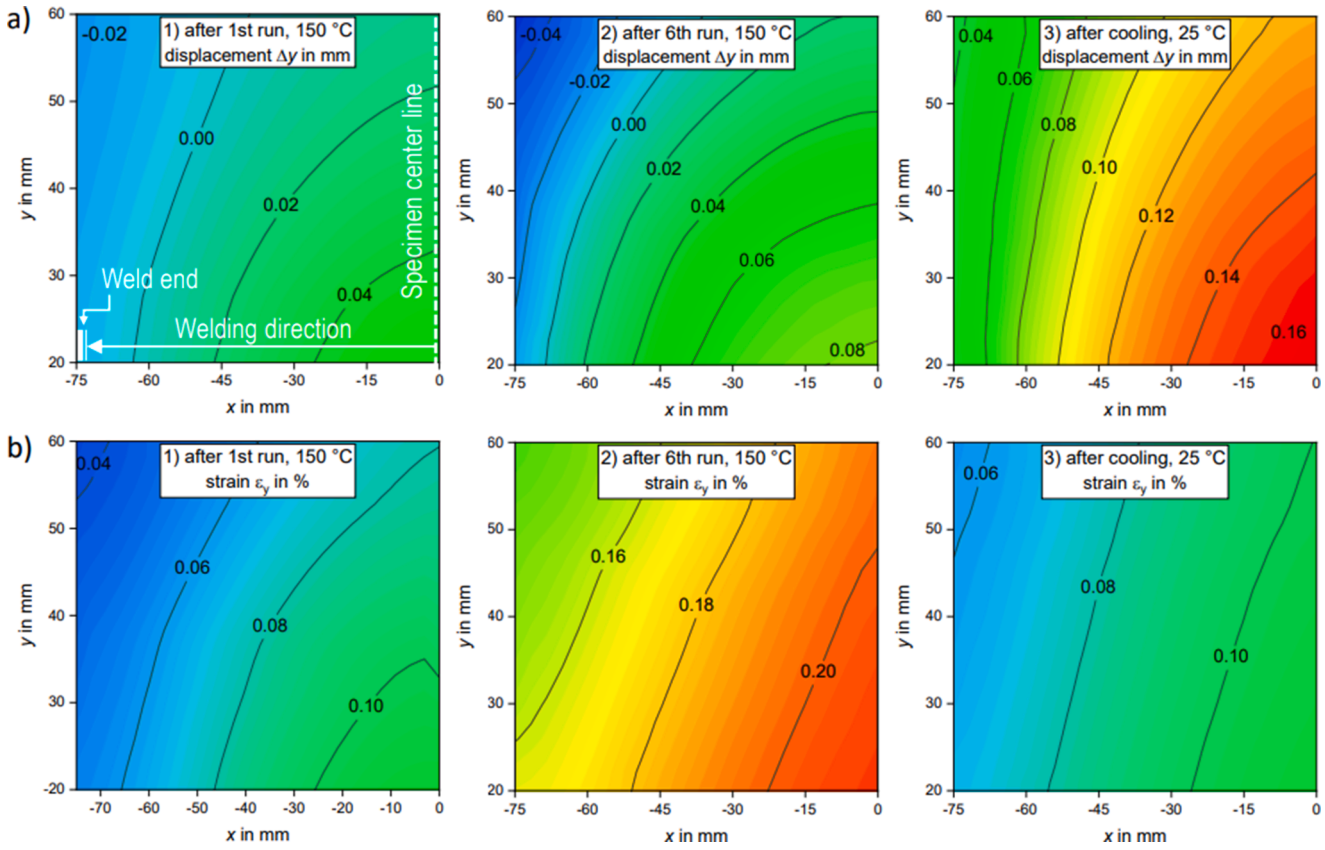

Fig. 7. (a) Maps of displacement Δy after 1st run (150 °C), 6th (last) run (150 °C) and after cooling to ambient temperature (25 °C), (b) Maps of strain ε_y after 1st run (150 °C), 6th (last) run (150 °C) and after cooling to ambient temperature (25 °C).

Declaration of Competing Interest

The authors declare no conflict of interest.

Acknowledgements

The IGF-project (IGF20162N) 'Appropriate repair of weld seams during manufacturing of high-strength fine-grain structural steel components' of the Research Association for Steel Application (FOSTA) was supported by the Federal Ministry for Economic Affairs and Energy by the AiF as part of the program for support of the cooperative industrial research (IGF) on the basis of a decision by the German Bundestag. Sincere thanks are given for this support and to the representing companies actively involved in the project board.

References

[1] T. Kannengiesser, Challenges when welding components made of higher-strength fine-grained structural steels, Weld. Cutt. 13 (2014) 384–392.
[2] European Standard EN 1011-2, Welding - Recommendation for Welding of Metallic Materials - Part 2: Arc Welding of Ferritic Steels, 2001.
[3] R. Schasse, T. Kannengiesser, A. Kromm, T. Mente, Residual stresses in repair welds of high-strength low-alloy steels, Weld. World 59 (2015) 757–765, https://doi.org/10.1007/s40194-015-0257-9.
[4] Ø. Grong, Metallurgical Modelling of Welding, 1997.
[5] M. Karpenko, Influence of the Cutting Gases During Thermal Cutting, Dissertation (in Gemarn), 2001.
[6] P.J. Withers, H.K.D.H. Bhadeshia, Overview - Residual stress Part 2 - Nature and origins, Mater. Sci. Technol. 17 (4) (2001) 366–375, https://doi.org/10.1179/026708301101510087.
[7] J. Sun, J. Hensel, T. Nitschke-Pagel, K. Dilger, Influence of restraint conditions on welding residual stresses in H-Type cracking test specimens, Materials 12 (17) (2019), https://doi.org/10.3390/ma12172700.
[8] D. Schroepfer, A. Kromm, T. Schaupp, T. Kannengiesser, Welding stress control in high-strength steel components using adapted heat control concepts, Weld. World 63 (3) (2018) 647–661, https://doi.org/10.1007/s40194-018-00691-z.
[9] D. Schroepfer, A. Kromm, T. Kannengiesser, Formation of multi-axial welding stresses due to material behaviour during fabrication of high-strength steel components, Weld. World 63 (1) (2018) 43–51, https://doi.org/10.1007/s40194-018-0650-2.
[10] K. Satoh, Y. Ueda, H. Kihara, Recent trends of research into restraint stresses and strains in relation to weld cracking, Weld.World 11 (1973) 133–156.
[11] Satoh K., Nakajima H., Toyosada M. (1972) Restraint intensity of weld joints in the structural members consisting of plates and stiffeners, IIW-Doc X-660-72.
[12] K. Masubuchi, Residual stresses and distortion. ASM Handbook; Vol. 6: Welding, ASM International, Brazing and Soldering, 1993.
[13] C. Schwenk, T. Kannengiesser, M. Rethmeier, Restraint conditions and welding residual stresses in self-restrained cold cracking tests, in: Trends in Welding Research: Proceedings of the 8th International Conference, ASM International, 2009, https://doi.org/10.1361/cp2008twr766.
[14] D. Schroepfer, A. Kromm, T. Lausch, M. Rhode, R.C. Wimpory, T. Kannengiesser, Influence of welding stresses on relief cracking during heat treatment of a creep-resistant 13CrMoV steel Part III: assessment of residual stresses from small-scale to real component welds, Weld. World 65 (9) (2021) 1671–1685, https://doi.org/10.1007/s40194-021-01101-7.
[15] D. Schroepfer, A. Kromm, T. Kannengiesser, Load analyses of welded high-strength steel structures using image correlation and diffraction techniques, Weld. World 62 (3) (2018) 459–469, https://doi.org/10.1007/s40194-018-0566-x.
[16] P. Dong, J.K. Hong, P.J. Bouchard, Analysis of residual stresses at weld repairs, Int. J. Press. Vessels Piping 82 (2005) 258–269, https://doi.org/10.1016/j.ijpvp.2004.08.004.
[17] P.J. Withers, H.K.D.H. Bhadeshia, Overview - Residual stress Part 1 - Measurement techniques, Mater. Sci. Technol. 17 (4) (2001) 355–365, https://doi.org/10.1179/026708301101509980.
[18] T. Nitschke-Pagel, H. Wohlfahrt, The generation of residual stresses due to joining processes. Residual stresses - measurement, calculation, evaluation, DGM Informationsgesellschaft mbH (1991). ISBN3-88355-169-4.
[19] T. Nitschke-Pagel, H. Wohlfahrt, Residual stresses in welded joints - sources and consequences, Mater. Sci. Forum 404 (407) (2002) 215–226, https://doi.org/10.4028/www.scientific.net/MSF.404-407.215.